17 April 2026

Stochastic Evaluation of Exciton–Exciton Annihilation Rate in 2D Molecular Aggregate

Chengyu Kuang[1,2], Dimitri Bazile[1], Chern Chuang[3], Daniel Neuhauser[1], Justin R. Caram[1]

1. Department of Chemistry and Biochemistry, University of California

2. St Edmund Hall, University of Oxford

3. Department of Chemistry and Biochemistry, University of Nevada

Abstract

Exciton-exciton annihilation (EEA) is a process by which two excitons combine to form a single high energy excitation. In molecular chromophore aggregates EEA is governed by microscopic two-exciton coherence that depends on long-range coupling and supramolecular geometry, motivating scalable quantum mechanical rate calculations beyond deterministic small-system diagonalization. Here, we develop a Fast Fourier Transform (FFT)-accelerated stochastic method for computing finite temperature EEA rates in large 2D excitonic molecular aggregates. We demonstrated agreement with conventional deterministic matrix diagonalization for small and intermediate systems, while achieving an improved scaling of $O(N^2 \log N)$ from $O(N^6)$ cost. This approach enables large-scale parameter sweeps and structure–function screening in realistic 2D morphologies. We close by exploring the role of uncorrelated and correlated disorder, temperature and inter-exciton coupling in EEA.

 https://doi.org/10.26434/chemrxiv.15002136/v1

Stochastic Evaluation of Exciton-Exciton Annihilation Rate in 2D Molecular Aggregates

Chengyu Kuang,[1,2] Dimitri Bazile,[1] Chern Chuang,[3] Daniel Neuhauser,[1,a)] and Justin R. Caram[1,b)]
[1)] *Department of Chemistry and Biochemistry, University of California, Los Angeles, 607 Charles E. Young Drive, Los Angeles, California 90095-1569, United States*
[2)] *St Edmund Hall, University of Oxford, Queen's Lane, Oxford, OX1 4AR, United Kingdom*
[3)] *Department of Chemistry and Biochemistry, University of Nevada, Las Vegas, Nevada 89154, United States*

(Dated: 15 April 2026)

Exciton-exciton annihilation (EEA) is a process by which two excitons combine to form a single high energy excitation. In molecular chromophore aggregates EEA is governed by microscopic two-exciton coherence that depends on long-range coupling and supramolecular geometry, motivating scalable quantum mechanical rate calculations beyond deterministic small-system diagonalization. Here, we develop a Fast Fourier Transform (FFT)-accelerated stochastic method for computing finite temperature EEA rates in large 2D excitonic molecular aggregates. We demonstrated agreement with conventional deterministic matrix diagonalization for small and intermediate systems, while achieving an improved scaling of $O(N^2 \log N)$ from $O(N^6)$ cost. This approach enables large-scale parameter sweeps and structure–function screening in realistic 2D morphologies. We close by exploring the role of uncorrelated and correlated disorder, temperature and inter-exciton coupling in EEA.

I. INTRODUCTION

Exciton-exciton annihilation (EEA) is a ubiquitous many-body relaxation pathway in which two photoexcitations interact such that one exciton is quenched while the other is promoted to a higher-lying excited state (Figure 1a).[1–3] In excitonic materials, EEA limits device performance by setting the maximum exciton density that a material can support, acting as a key loss channel in high light applications such as organic thin-film lasers and organic light-emitting diodes.[4–6] EEA is also a useful diagnostic, where the power-dependent EEA can be used to infer exciton diffusion and interaction lengths from ultrafast spectroscopy.[6–8]

In the coarse-grained macroscopic description, EEA appears as a bimolecular loss term in the exciton-density rate equation:[9,10]

$$\frac{dn}{dt} = -\frac{n}{\tau} - \gamma n^2 \; ; \quad \Gamma = \gamma n^2, \tag{1}$$

where n is the exciton density, Γ is the EEA rate, γ is the EEA rate constant, and τ is the intrinsic exciton lifetime without the presence of other excitons. Quantitative modeling and materials design therefore hinge on predicting the annihilation rate under realistic morphology, static disorder, and vibronic relaxation.[11,12] This need has motivated a broad hierarchy of simulation approaches.

On a simplified level, EEA can be treated as an incoherent, diffusion-limited encounter process in which excitons are modeled as classical particles with a diffusion constant D, and annihilation occurs when two excitons come within an annihilation radius R_0.[13–15] On the contrary, microscopic, electronic-structure–informed approaches treat EEA as an inelastic quantum transition in which the two-exciton (S_1–S_1) manifold couples to higher-lying single-exciton states (S_n), with coherence and interference modulating the annihilation rate.[16] This is particularly important for Frenkel excitons in molecular aggregates, where delocalization and phase structure can qualitatively reshape EEA,[17,18] so that the bimolecular EEA rate is governed by quantum-mechanical transition matrix elements rather than a random walk model with an encounter radius. In particular, wavefunction interference can coherently suppress annihilation in H-aggregates in comparison to J-aggregates in 1D systems, so purely diffusive pictures that assume localized, incoherent excitons can miss the dominant physics and even predict incorrect trends.[6,19–24] At the higher end of the methodology hierarchy, a full quantum dynamical treatment based on open-system master equations on density matrix can, in principle, include bath interactions and vibronic relaxation; however, its cost grows rapidly with aggregate size and bath complexity, making such approaches impractical for micrometer-scale 2D aggregates.[1,25–28] Recent stochastic bundling schemes can reduce this cost significantly, but full density-matrix propagation remains too expensive for truly large 2D aggregates.[29]

Motivated by the need to retain coherent Frenkel-exciton physics at experimentally relevant length scales while remaining computationally affordable, one can adopt a Fermi's golden rule (FGR) description, in which vibrational relaxation enters through an effective density-of-states factor.[6,23,30,31] In this framework, the two-exciton manifold is assumed to thermalize before EEA,

[a)] Electronic mail: dxn@ucla.edu
[b)] Electronic mail: jcaram@ucla.edu

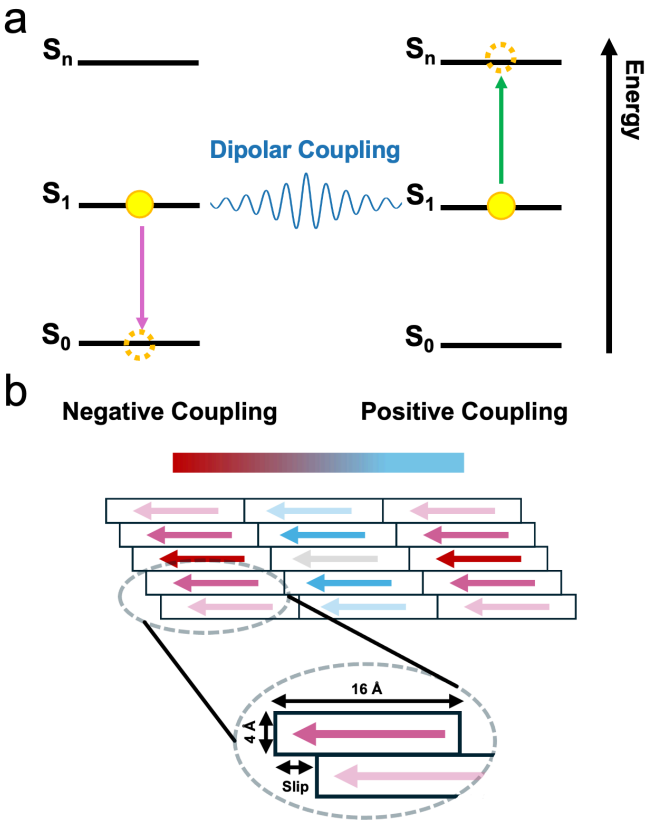

FIG. 1. (a) Illustration of exciton–exciton annihilation (EEA) in molecular aggregates. Two excitons localized on neighboring chromophores interact through dipole–dipole coupling, forming a two-exciton state that undergoes EEA. One chromophore relaxes to the ground state while the other is promoted to a higher excited state S_n, followed by rapid thermal relaxation back to S_1. (b) Diagram of a section of a 2D planar aggregate. The relative excitonic coupling strengths between a reference chromophore monomer (white) and its nearest neighbors are indicated by different colors. The slip between adjacent molecules controls the sign and magnitude of the dipole–dipole interaction.

while the annihilation process itself is treated perturbatively. However, even at the FGR level, the computational bottleneck remains severe for non-1D aggregates with non-nearest-neighbor couplings. The finite-temperature rate requires thermal averaging over matrix elements in the hard-core two-exciton manifold. In standard state-resolved formulations, this entails constructing and diagonalizing a dense two-exciton Hamiltonian whose dimension scales as $O(N^2)$ and whose diagonalization cost scales $O(N^6)$, where N is the number of monomers, before disorder averaging.[23]

This difficulty is exacerbated by long-range dipole–dipole couplings ($J \propto r^{-3}$), which leads to slow convergence with regard to interaction cutoff—particularly in 2D and quasi-2D (e.g. tubular) aggregates where very large lattices are needed to tame finite-size effects.[32–34] Moreover, the physically relevant two-exciton manifold is restricted by the hard-core constraint ($n_1 \neq n_2$, where n_1 and n_2 denote the monomer indices occupied by the two excitons) and can be further modified by exciton–exciton binding interactions. As a result, the dynamics cannot, in general, be reduced to products of separable one-exciton problems.[35] Although methods like Jordan–Wigner transformations can simplify hard-core many-body problem into terms of factorized one particle wavefunctions in special one-dimensional nearest-neighbor models, this simplification does not extend to the present two-dimensional system with long-range couplings.[36,37]

We addressed this bottleneck by casting the finite-temperature FGR EEA rate for 2D molecular aggregates as a thermal trace over the hard-core two-exciton manifold, and then estimating that trace with stochastic vectors.[38–40] We further exploited the translational symmetry of lattice structure through Fast Fourier Transform (FFT) based acceleration, which enables us to avoid explicit matrix multiplication and diagonalization.[38,41] This reformulation eliminates the need to construct two-exciton eigenstates or to explicitly form the dense two-particle Hamiltonian, while still retaining the wavefunction phase information. More generally, the same formalism is not restricted to EEA-rate calculations and could potentially be extended to other numerically challenging many-exciton processes, such as excited-state absorption, correlated triplet-pairs generated from singlet fission, charge separation dynamics, and higher order electronic spectroscopy.[42–48] This makes it feasible to work in the molecular aggregates regime where (i) long-range couplings cannot be ignored, and (ii) disorder, exciton-exciton interactions, and thermal sampling are essential.[32,33,38]

We validated the approach against deterministic diagonalization on small lattices, showing rapid and systematic convergence with both the splitting operation steps and the number of stochastic vectors used. Once benchmarked, the same pipeline becomes a reliable screening tool with controlled numerical precision. We can efficiently map how Γ varies across aggregates with different slip and quantify how temperature, uncorrelated and correlated static disorder, and explicit exciton–exciton interactions reshape annihilation. In this way, the stochastic-trace formulation provides a scalable, coherence route to connect microscopic Hamiltonians to experimentally relevant annihilation rate, enabling parameter studies that are effectively out of reach for traditional state-resolved two-exciton methods.

II. METHODS

Model and Hamiltonians

We considered a 2D aggregate with $N = N_x N_y$ chromophore monomers on a periodic $N_x \times N_y$ lattice. In the site basis $\{|n\rangle\}_{n=1}^{N}$, the one-particle Frenkel exciton

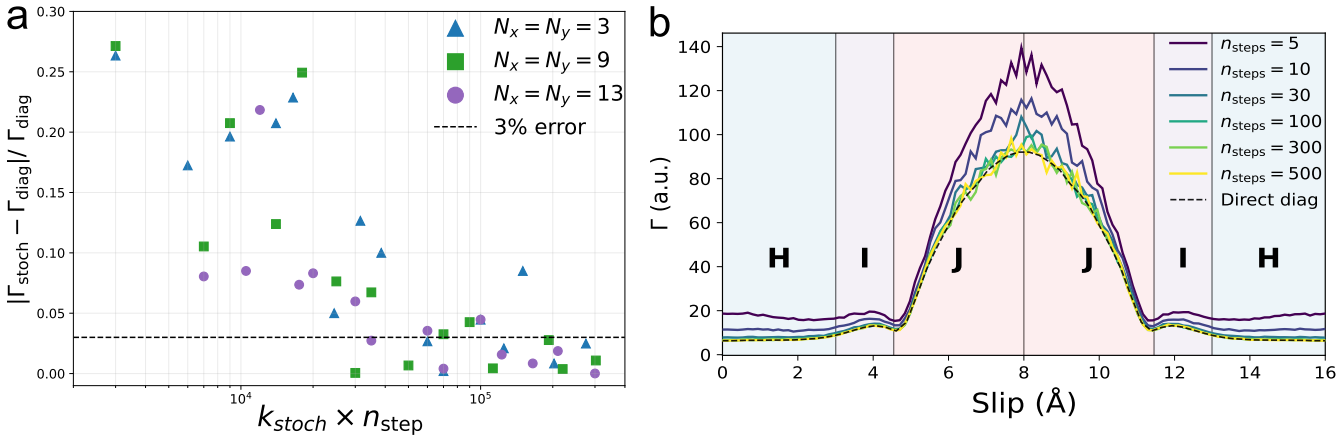

FIG. 2. Convergence and parameter screening of the stochastic EEA rate. (a) Convergence of the stochastic estimate of the EEA rate toward the deterministic reference at slip = 0 Å, shown as a function of $k_{\mathrm{stoch}} n_{\mathrm{step}}$ for aggregates of increasing size: $N_x = N_y = 3$, $N_x = N_y = 9$, and $N_x = N_y = 13$. The dashed black line indicates the 3% error level. (b) Slip dependence of the annihilation rate computed with the stochastic method for different propagation steps, n_{step} (solid lines), with $k_{\mathrm{stoch}} = 300$ and $N_x = N_y = 11$, showing convergence toward the deterministic reference (dashed line). The temperature is fixed at $T = 300$K.

Hamiltonian is:[49–52]

$$\hat{H}_1 = \sum_{n=1}^{N} \epsilon_n |n\rangle\langle n| + \sum_{n\neq m}^{N} J_{nm} |n\rangle\langle m|, \tag{2}$$

here, ϵ_n is the site energy of monomer n and J_{nm} is the electronic coupling between monomers n and m. To model static energetic disorder, we wrote

$$\epsilon_n = \epsilon_0 + \delta\epsilon_n, \tag{3}$$

where ϵ_0 is the monomer (S_0–S_1) transition energy and $\delta\epsilon_n$ is a static random disorder. In this work, we chose the energy reference such that $\epsilon_0 = 0$.

For uncorrelated random disorder, it was sampled independently from a Gaussian distribution,

$$\delta\epsilon_n \sim \mathcal{N}(0, \sigma^2), \qquad \mathrm{Cov}(\delta\epsilon_n, \delta\epsilon_m) = \sigma^2 \delta_{nm}, \tag{4}$$

where σ is the disorder standard deviation. For correlated random disorder, we assumed an exponentially decaying spatial covariance,

$$\mathrm{Cov}(\delta\epsilon_n^{\mathrm{corr}}, \delta\epsilon_m^{\mathrm{corr}}) = \sigma^2 \exp\left(-\frac{r_{nm}}{R_c}\right), \tag{5}$$

where r_{nm} is the intermolecular separation on the periodic lattice and R_c is the disorder correlation length. For a perfect 2D lattice, such correlated random disorder can be generated efficiently by Fourier-space filtering. Writing the covariance kernel as $\mathrm{Cov}^{\mathrm{corr}}(\mathbf{r})$ and its discrete 2D Fourier transform as $\widetilde{\mathrm{Cov}}^{\mathrm{corr}}(\mathbf{k})$, one realization is obtained as[53]

$$\delta\epsilon^{\mathrm{corr}} = F^{-1}\left[\sqrt{\widetilde{\mathrm{Cov}}^{\mathrm{corr}}(\mathbf{k})}\, F[\delta\epsilon]\right], \tag{6}$$

which ensures that the sampled disorder has the target covariance in Eq. (5).

We considered transition dipole coupling as the dominant intermolecular coupling between chromophore monomers. We employed the extended dipole model to compute the electronic coupling. Each chromophore monomer is represented by two opposite charges separated by a fixed distance d along the transition dipole direction. The intermolecular coupling is then obtained as the Coulomb interaction between the two pairs of charges defining the two extended dipoles,[54]

$$J_{\mathrm{ext}} = \xi q^2 \left(\frac{1}{r_{++}} + \frac{1}{r_{--}} - \frac{1}{r_{+-}} - \frac{1}{r_{-+}}\right), \tag{7}$$

where $r_{m\pm,n\pm}$ denotes the distance between the indicated charges on chromophore monomer m and n, q is the magnitude of the effective transition charge, and ξ carries the unit-conversion constant.

For a perfect 2D lattice with periodic boundary conditions and without disorder, J_{nm} depends only on the relative displacement and $\hat{H}_1$ is a block-circulant matrix with circulant blocks (BCCB), hence diagonalized by a 2D discrete Fourier transform,

$$\hat{H}_1 = F^{-1} \Lambda F, \tag{8}$$

with the eigenvalue array given by the 2D Fourier transform of the kernel,

$$\lambda = F[K], \tag{9}$$

where K is the real-space kernel of $\hat{H}_1$, F denotes the two-dimensional discrete Fourier transform on the (N_x, N_y) lattice, and $\Lambda = \mathrm{diag}(\lambda)$.

We wrote the two-exciton Hamiltonian as

$$\hat{H}_2 = \hat{H}_1 \otimes I + I \otimes \hat{H}_1 + \hat{V}, \tag{10}$$

where $\hat{H}_1 \otimes I + I \otimes \hat{H}_1$ is represented in the hard-core two-exciton basis space M, and both it and the exciton–exciton interaction operator $\hat{V}$ are defined below.

Finite-temperature FGR rate with stochastic vectors

A Fermi's golden rule expression for the annihilation rate can be written as:[6]

$$\Gamma(T) = \frac{2\pi}{\hbar\,\gamma_{\mathrm{vib}}} \sum_{\lambda} P_\lambda \sum_{m} \left| \left\langle S_\alpha(m) \left| \hat{H}_a \right| \Psi_\lambda \right\rangle \right|^2, \quad (11)$$

where γ_{vib} is the vibrational relaxation rate constant of the final localized higher-lying singly excited S_n states produced after EEA, $\{|\Psi_\lambda\rangle\}$ are eigenstates of $\hat{H}_2$, $P_\lambda \propto e^{-\beta E_\lambda}$ are the corresponding thermal populations, and $\{|S_\alpha(m)\rangle\}$ denote the final single exciton high energy states accessed through the annihilation operator $\hat{H}_a$.[55] The latter is written as:[6]

$$\hat{H}_a = \sum_{n \neq m} V_{n,m}\, b_m^\dagger b_m b_n + \mathrm{H.c.}, \quad (12)$$

where $V_{n,m}$ denotes the resonant coupling between the $S_1 - S_n$ and $S_0 - S_1$ transitions on chromophores n and m, respectively, and $b_m^\dagger$ (b_m) is the exciton creation (annihilation) operator on chromophore m.[6] In this study, the couplings entering $\hat{H}_a$ are assumed to have the same dipolar form as the single-exciton couplings, with $V_{n,m} = \eta J_{n,m}$, where η is a constant prefactor.[6]

The thermally averaged EEA rate can be expressed as a ratio of thermal traces over the hard-core two-exciton manifold:

$$\Gamma(T) = \frac{2\pi}{\hbar\,\gamma_{\mathrm{vib}}} \frac{\mathrm{Tr}\left(e^{-\beta \hat{H}_2}\, \hat{H}_a^\dagger \hat{H}_a\right)}{\mathrm{Tr}\left(e^{-\beta \hat{H}_2}\right)}, \qquad \beta = (k_B T)^{-1}. \quad (13)$$

Let $\mathcal{H}_2^{(\mathrm{hc})}$ denote the hard-core two-exciton state space of dimension

$$M = \frac{N(N-1)}{2}. \quad (14)$$

For any operator $\hat{A}$ on $\mathcal{H}_2^{(\mathrm{hc})}$, stochastic vector sampling yields an unbiased trace estimator: [38–40]

$$\mathrm{Tr}(\hat{A}) \approx \frac{1}{k_{\mathrm{stoch}}} \sum_{k=1}^{k_{\mathrm{stoch}}} \langle \chi_k | \hat{A} | \chi_k \rangle, \quad (15)$$

where $|\chi_k\rangle$ is a random vector.

Define, for each probe,

$$|v_k\rangle = e^{-(\beta/2)\hat{H}_2}\, |\chi_k\rangle. \quad (16)$$

Then the per-probe denominator and numerator contributions are

$$t_{\mathrm{den}}^{(k)} = \langle v_k | v_k \rangle, \qquad t_{\mathrm{num}}^{(k)} = \langle v_k | \hat{H}_a^\dagger \hat{H}_a | v_k \rangle = \| \hat{H}_a v_k \|^2, \quad (17)$$

and the rate estimate is

$$\Gamma(T) \approx \frac{2\pi}{\hbar\,\gamma_{\mathrm{vib}}} \frac{\frac{1}{k_{\mathrm{stoch}}} \sum_{k=1}^{k_{\mathrm{stoch}}} t_{\mathrm{num}}^{(k)}}{\frac{1}{k_{\mathrm{stoch}}} \sum_{k=1}^{k_{\mathrm{stoch}}} t_{\mathrm{den}}^{(k)}}. \quad (18)$$

Projected split-operator propagation and FFT acceleration

The main numerical task is the repeated application of $e^{-(\beta/2)\hat{H}_2}$ without explicitly forming or diagonalizing $\hat{H}_2$(of which scales as $O(N^6)$ for the computational cost). We approached $\hat{H}_2$ using a splitting operation by embedding a hard-core pair state into an $N \times N$ matrix Φ on the full tensor-product space, applying FFT-accelerated left and right actions induced by $\hat{H}_1 \otimes I$ and $I \otimes \hat{H}_1$, and projecting with the constraint operator $\hat{C}$ after each substep. Using Eq.(8), the exponentials are implemented as

$$e^{-t(\hat{H}_1 \otimes I)}\Phi = F^{-1} e^{-t\Lambda} F\, \Phi, \quad (19)$$

$$e^{-t(I \otimes \hat{H}_1)}\Phi = \Phi\, F^{-1} e^{-t\Lambda} F. \quad (20)$$

Write $\hat{H}_2 = \hat{L} + \hat{R} + \hat{V}$ with $\hat{L} = \hat{H}_1 \otimes I$ and $\hat{R} = I \otimes \hat{H}_1$. For a step size $\Delta\tau$, we used a splitting operation

$$e^{-\Delta\tau \hat{H}_2} \approx \hat{C} e^{-(\Delta\tau/2)\hat{V}}\, e^{-(\Delta\tau/2)\hat{L}}\, e^{-\Delta\tau \hat{R}}\, e^{-(\Delta\tau/2)\hat{L}}\, e^{-(\Delta\tau/2)\hat{V}}\, \hat{C}, \quad (21)$$

where $\hat{C}$ is a projection operator which removes all diagonal amplitudes and enforces the exchange symmetry when $e^{-\Delta\tau \hat{H}_2}$ acts on a two-exciton wavevector with an N^2 dimension. Repeating n_{step} steps with $\Delta\tau = \beta/(2n_{\mathrm{step}})$ yields $e^{-(\beta/2)\hat{H}_2}$.

Exciton–exciton interaction

We used a Hubbard-type exciton–exciton diagonal interaction where the interactions are proportional to the underlying single-exciton coupling:[56–58]

$$\hat{V} = \sum_{n<m} \kappa\, J_{nm}\, |n,m\rangle\langle n,m|. \quad (22)$$

$$e^{-\Delta\tau \hat{V}} |n,m\rangle = e^{-\Delta\tau\, \kappa J_{nm}} |n,m\rangle. \quad (23)$$

Full algorithm

The pseudocode for the $\Gamma(T)$ sampling procedure is given in Algorithm 1.

Scaling and Error analysis

Each splitting operation step requires a constant number of FFT-based left/right multiplications. Since the propagated object is an $N \times N$ matrix embedding the $O(N^2)$ hard-core manifold, the dominant cost is $O(N^2 \log N)$ per propagation step, giving total wall-time

$$\mathrm{cost} \sim O\big(k_{\mathrm{stoch}}\, n_{\mathrm{step}}\, N^2 \log N\big), \quad (24)$$

Algorithm 1 Pseudocode for $\Gamma(T)$ generation

Construct the disorder-free BCCB part $\hat{H}_1^{(0)}$ on an (N_x, N_y) lattice using extended dipole couplings J_{nm} and periodic boundary conditions.
Exploit the BCCB structure of $\hat{H}_1^{(0)}$ to obtain $\Lambda = F[K]$.
Set $\beta = (k_B T)^{-1}$, choose n_{step}, and define

$$\Delta\tau = \beta/(2n_{\text{step}}).$$

for $k = 1, \ldots, k_{\text{stoch}}$ **do**
    Draw a random vector $\chi_k \in \mathbb{C}^M$.
    Draw a random site-disorder realization and define

$$\hat{D}_k = \sum_{n=1}^{N} \delta\epsilon_n^{(k)} |n\rangle\langle n|$$

    Initialize $\Psi \leftarrow \chi_k$.
    for $m = 1, \ldots, n_{\text{step}}$ **do**
        Unpack Ψ into an $N \times N$ off-diagonal matrix Φ.
        Apply left half-step with inner disorder splitting:

$$\Phi \leftarrow e^{-(\Delta\tau/4)\hat{D}_k}\, F^{-1} e^{-\Delta\tau\Lambda/2} F\, e^{-(\Delta\tau/4)\hat{D}_k}\, \Phi,$$

        then project with $\hat{C}$.
        Apply interaction half-step:

$$\Phi \leftarrow e^{-(\Delta\tau/2)\hat{V}} \Phi.$$

        then project with $\hat{C}$.
        Apply right full-step with inner disorder splitting:

$$\Phi \leftarrow \left(\Phi\, e^{-(\Delta\tau/2)\hat{D}_k}\right) F^{-1} e^{-\Delta\tau\Lambda} F\, e^{-(\Delta\tau/2)\hat{D}_k}.$$

        then project with $\hat{C}$.
        Apply interaction half-step:

$$\Phi \leftarrow e^{-(\Delta\tau/2)\hat{V}} \Phi.$$

        then project with $\hat{C}$.
        Apply the left half-step again:

$$\Phi \leftarrow e^{-(\Delta\tau/4)\hat{D}_k}\, F^{-1} e^{-\Delta\tau\Lambda/2} F\, e^{-(\Delta\tau/4)\hat{D}_k}\, \Phi,$$

        then project with $\hat{C}$.
        Pack Φ back into the pair vector Ψ.
    end for
    Set $v_k \leftarrow \Psi$.
    Update

$$S_{\text{den}} \leftarrow S_{\text{den}} + \|v_k\|^2, \qquad S_{\text{num}} \leftarrow S_{\text{num}} + \|\hat{H}_a v_k\|^2.$$

end for
Return

$$\Gamma(T) = \frac{2\pi}{\hbar\,\gamma_{\text{vib}}} \frac{S_{\text{num}}}{S_{\text{den}}}.$$

in contrast to the $O(N^6)$ scaling implied by explicit construction and diagonalization in the $M \sim O(N^2)$ two-exciton Hilbert space.

For the disorder-free case, the numerical error of the stochastic splitting estimator can be decomposed as

$$\begin{aligned} \Gamma_{k_{\text{stoch}},\, n_{\text{step}}}(T) &= \Gamma(T) + \delta\Gamma_{\text{stoch}} + \delta\Gamma_{\text{split}}, \\ \delta\Gamma_{\text{stoch}} &= O\left(k_{\text{stoch}}^{-1/2}\right), \delta\Gamma_{\text{split}} = O\left(n_{\text{step}}^{-2}\right), \end{aligned} \tag{25}$$

here $\delta\Gamma_{\text{stoch}}$ comes from the finite number of random vectors used in the stochastic trace estimator, giving the standard Monte Carlo error scaling[59]. The term $\delta\Gamma_{\text{split}}$ comes from the finite-step second order splitting operation of the propagator $e^{-(\beta/2)\hat{H}_2}$, which is globally second-order accurate in $\Delta\tau$.[60]

III. RESULTS AND DISCUSSION

EEA in 2D cyanine dye aggregate sheets was studied using the aforementioned formalism, with detailed parameters and geometrical setup described in the Supporting Information(SI) section 3.[61] Figure 1b showed the geometric setup for the 2D molecular aggregate system, with the slip controlling the coupling patterns.

To highlight the accuracy of the stochastic methods, we compared the EEA rate across different systems sizes with deterministic approaches based on matrix diagonalization (more in SI section 1) shown in Figure 2a. By systematically varying k_{stoch} and n_{step}, we found that $k_{\text{stoch}} = 300$ and $n_{\text{step}} = 300$ are sufficient to achieve convergence at slip = 0. Detailed individual analysis on the convergence on both n_{step} and k_{stoch} can be found in SI section 2. Next, we tested the convergence with increasing n_{step} and fixed $k_{\text{stoch}} = 300$ across different slip values, as shown in Figure 2b. The larger n_{step} required in the range of 6–10 Å was likely due to the larger ratio between horizontal and longitudinal J-couplings, which increases the splitting-operation error and therefore necessitates more splitting steps.

Interestingly, the EEA rate reached a turning point near the boundary between I/J aggregates. Very briefly, for 2D chromophore aggregates, the I-aggregate region is defined as when the bright exciton is redshifted from the monomer but not the lowest energy state, while the J-aggregate bright state is pinned to the band-edge (details in SI section 4).[61] This crossover marked the point where the positive short-range coupling is nearly canceled by the always-negative long-range contribution close to the bright state ($\vec{k} = 0$) at the bottom of the band. This leds to a flattened exciton band near it as well as minimal exciton bandwidth (Detailed discussion on the classifications of H/I/J on the current system based on the single exciton band can be found in SI section 4). In the EEA rate expression [Eq.(8) in the SI] Γ is governed by coherent sums of the form $\sum_{n>m} \alpha J_{m,n}\, C_\lambda(m,n)$; near the I/J edge, the competing signs and reduced magnitude of the couplings enhanced destructive cancellation in these annihilation matrix elements, thereby suppressing the rate. Moving further into the J-aggregate regime, the relevant couplings become more uniformly negative, as indicated

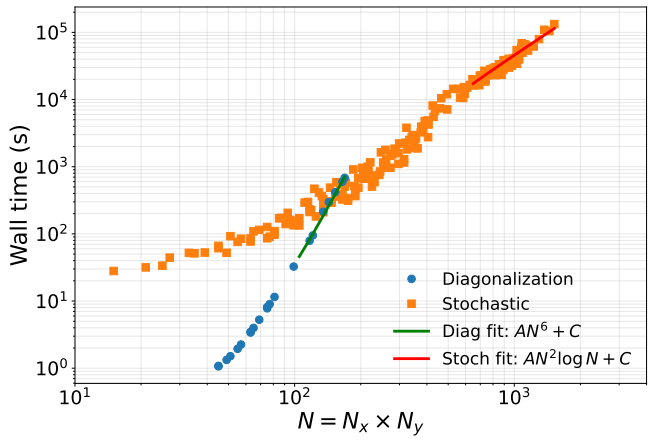

FIG. 3. Computational scaling of EEA rate evaluation. Wall-time scaling of the EEA rate calculation as a function of number of monomers. Measured runtimes for direct diagonalization and the stochastic FFT-based method(with $k_{\text{stoch}} = 300$ and $n_{\text{step}} = 300$) are shown as symbols. Solid lines indicate fits to the scaling law predictions. All timings were obtained on a AMD EPYC 9654 CPU (192 cores per CPU), and the times recorded are single core time.

by the larger bandwidth. Therefore, the coherent sums add more constructively and the EEA rate increased.

We next benchmarked the computational cost of this methodology. Figure 3 compares the wall-time scaling of deterministic direct diagonalization and the stochastic FFT method as a function of system size $N = N_x N_y$. While deterministic direct diagonalization exhibited a steep N^6-like growth due to the size of the two-exciton Hilbert space, the stochastic FFT approach followed a much milder $N^2 \log N$ scaling. The widening separation with increasing N highlighted the clear computational advantage of the stochastic method for large systems. In particular, the stochastic approach enabled calculations for aggregates containing more than 1500 monomers, which are beyond the practical reach of deterministic direct diagonalization.

We next performed a multi-parameter screening of EEA rates. Disorder modifies exciton delocalization, coherence, and spectrum, and therefore alters the one- to two-exciton overlaps that control annihilation. [62,63] This is particularly important in 2D aggregates, where disorder have been shown to strongly affect excitonic observables and transport-related behavior.[64] In the present stochastic framework, however, disorder averaging was incorporated directly into the estimator: each stochastic sample simultaneously drew a diagonal-disorder realization and a random vector, so the disorder-averaged EEA rate was obtained without introducing a separate expensive ensemble-averaging loop.[38]

Figure 4a reports the EEA rate under uncorrelated random disorder. Overall, this type of disorder leads to only relatively modest variations in the annihilation rate at room temperature, in line with the findings of Tempelaar *et al.*[6]

Figure 4b shows the slip dependence of the EEA rate as a function of temperature. As the temperature increased, the EEA rate of H-aggregates increases, while that of J-aggregates is suppressed. This behavior arises because, in the two-exciton eigenstate basis, increasing temperature reduced the weight of destructively interfering ground states in H-aggregates, while also diminishing the fully constructive contributions of ground states in J-aggregates.

Exciton-exciton interactions also plays an important role in determining EEA dynamics in molecular aggregates.[56,65] Biexcitonic interactions modify the energies and spatial profiles of two-exciton states. We therefore examined how the EEA rate varies with the exciton-exciton interaction providing insight into how many-body excitonic interactions reshape annihilation processes in extended aggregates.

Figure 4c shows the EEA rate as a function of slip and exciton–exciton interaction strength κ, indicating that the EEA rate increases significantly within the J-aggregate regime. We attributed this behavior to favorable exciton–exciton binding induced by the attractive coupling in the band-edge states of J-aggregates, forming gap states with bound biexcitons.[56] Within the present model, the biexciton binding energy in J-aggregates effectively restricts thermal access to higher energy two-exciton states and consequently induces higher EEA rate. On the other hand, the gap states of J-aggregates are buried in the two-exciton band in H-aggregates, and in the latter the EEA showed mild suppression with increasing κ. More details on the biexciton spectrum with finite κ is provided in the SI section 5.

In addition to the magnitude of energetic disorder shown in Figure 4a, its spatial correlation is expected to play an important role in excitonic dynamics in molecular aggregates.[18] Experimental and theoretical studies of excitonic molecular systems have suggested that environmental fluctuations can be spatially correlated across multiple chromophores.[53,66,67] In particular, quantum coherences with correlated system fluctuations have been observed in several multichromophoric systems, including semiconductor quantum dots and photosynthetic complexes, suggesting that relevant correlation length scales can extend over subnanometer distances comparable to intermolecular separations.[68,69] Such correlations may arise from collective phonon modes, defects on monomers, or correlated solvent fluctuations.[66,70] Consequently, examining the effect of correlated disorder on exciton–exciton annihilation (EEA) provides insight into exciton transport and interaction.

In Figure 4d, we investigated the effect of spatially correlated energetic disorder on the EEA rate by mapping the EEA rate across different correlation lengths for the disorder. In contrast to the weak dependence observed for purely uncorrelated random disorder in Figure 4c, the resulting map shows that the EEA rate depended strongly on the correlation length even when the over-

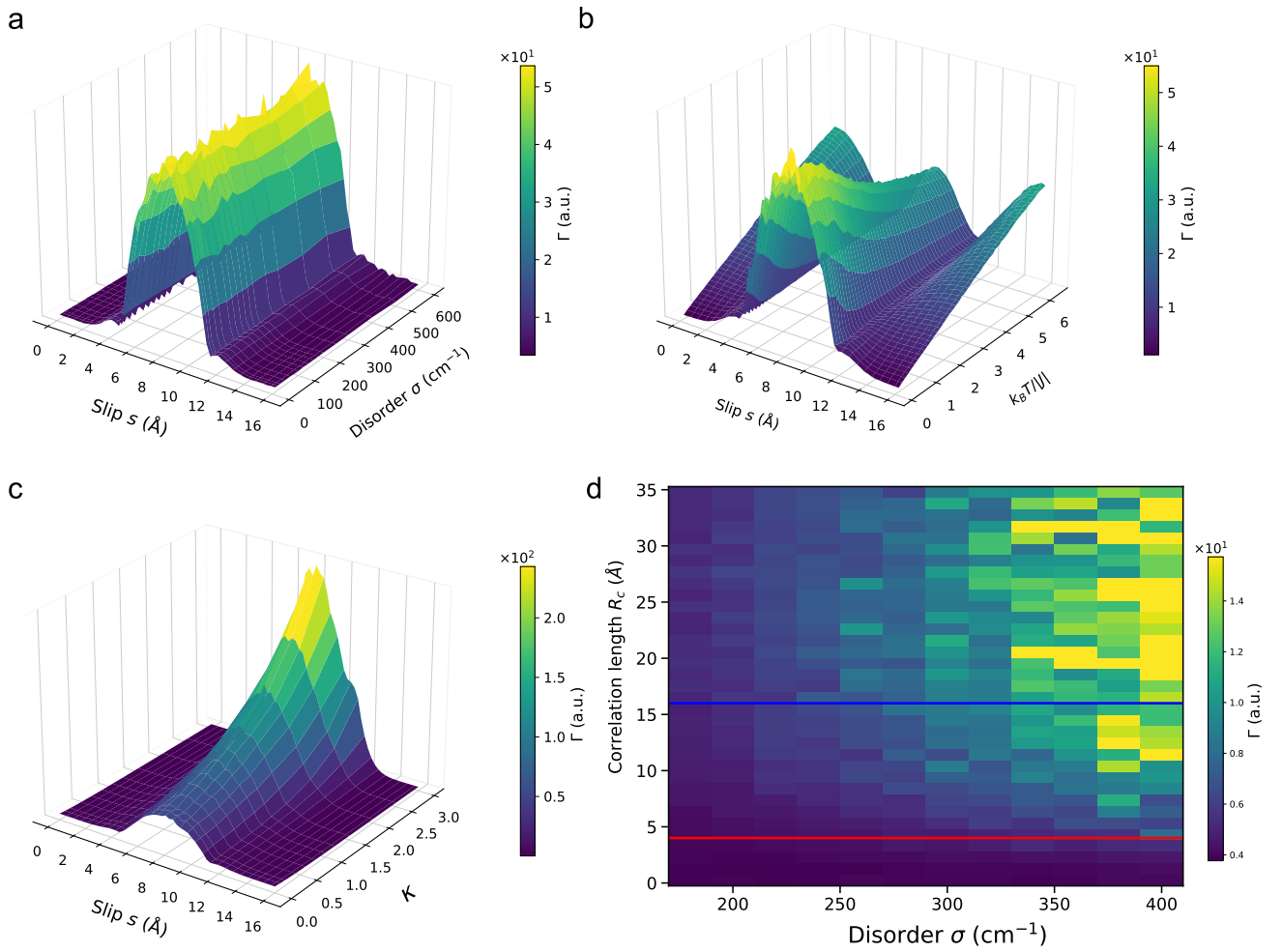

FIG. 4. Parameter screening of the EEA rate using stochastic evaluation. (a) EEA rate Γ illustrating the effect of uncorrelated random diagonal disorder strength. (b) EEA rate Γ showing the dependence of the annihilation rate on slip and temperature, with J denotes the nearest neighbor coupling along the transition dipole direction. (c) EEA rate Γ as a function of slip s and exciton–exciton interaction strength κ. (d) Heatmap of EEA rate Γ with slip = 0 Å illustrating the effect of special correlated diagonal disorder strength, the red and blue solid line indicate the width and the length of a single monomer respectively. All results were computed using $k_{\text{stoch}} = 300$ and $n_{\text{step}} = 300$. The aggregate size are all $N_x = N_y = 15$. The temperature is set to be T= 300K except for (b).

all disorder strength is held fixed. In particular, correlation lengths extending over only a few monomers can significantly increase the EEA rate, suggesting that short-range correlations create locally favorable and unfavorable energetic domains. This can draw excitonic amplitude into the same or neighboring favorable regions, effectively pushing excitons closer together in real space and hence increase EEA rate. This interpretation is consistent with recent work showing that spatially correlated site-energy disorder can create correlated low- and high-energy domains that reorganize exciton localization and trapping in molecular aggregates.[71]

IV. CONCLUSION

We developed a theoretical framework that enables the efficient treatment of large biexcitonic Hilbert spaces that are otherwise computationally prohibitive with conventional matrix diagonalizations. By replacing explicit construction and diagonalization of the two-exciton Hamiltonian with stochastic trace estimation and FFT-accelerated propagators, the computational scaling is reduced from approximately $O(N^6)$ to $O(N^2 \log N)$.

This efficient stochastic framework enabled systematic exploration of the biexcitonic parameter space in large molecular aggregates. By screening lattice slip, exciton–exciton interaction strength, temperature, and both random and correlated energetic disorder, we revealed how these factors reshape the excitonic landscape gov-

erning EEA.

Future work will extend this stochastic framework to study biexciton physics such as absorption spectra and density of states using Chebyshev expansion and stochastic sampling as demonstrated in previous study.[38] We will also investigate how optical cavities modify EEA using stochastic cavity methods.[41] Finally, the Hamiltonian splitting approach will allow efficient real-time propagation of two-exciton wave packets to compute time-dependent EEA dynamics, beyond the current Fermi's golden rule regime.

ACKNOWLEDGMENTS

CK and JRC were supported by the National Science Foundation under award number NSF-CHE-2506132. CC acknowledges the support by the National Science Foundation under award number NSF-CHE-2431226 and that of the University of Nevada, Las Vegas. DN acknowledges the support by the National Science Foundation (NSF) under Grant No. CHE-2245253. CK would like to acknowledge the helpful discussion with Yangzhou Xia.

AUTHOR DECLARATIONS

Conflict of interest

The authors have no conflicts to declare.

DATA AVAILABILITY

The data that support the findings of this study are available from the corresponding author upon reasonable request.

[1]B. Brüggemann, J. L. Herek, V. Sundström, T. Pullerits, and V. May, "Microscopic theory of exciton annihilation: Application to the LH2 antenna system," The Journal of Physical Chemistry B **105**, 11391–11394 (2001).

[2]D. Sun, Y. Rao, G. A. Reider, G. Chen, Y. You, L. Brézin, A. R. Harutyunyan, and T. F. Heinz, "Observation of rapid exciton–exciton annihilation in monolayer molybdenum disulfide," Nano letters **14**, 5625–5629 (2014).

[3]V. Malyshev, H. Glaeske, and K.-H. Feller, "Exciton–exciton annihilation in linear molecular aggregates at low temperature," Chemical physics letters **305**, 117–122 (1999).

[4]M. Baldo, R. Holmes, and S. Forrest, "Prospects for electrically pumped organic lasers," Physical Review B **66**, 035321 (2002).

[5]S. Z. Uddin, E. Rabani, and A. Javey, "Universal inverse scaling of exciton–exciton annihilation coefficient with exciton lifetime," Nano Letters **21**, 424–429 (2020).

[6]R. Tempelaar, T. L. Jansen, and J. Knoester, "Exciton–exciton annihilation is coherently suppressed in H-Aggregates, but not in J-aggregates," The journal of physical chemistry letters **8**, 6113–6117 (2017).

[7]J. D. Lin, O. V. Mikhnenko, J. Chen, Z. Masri, A. Ruseckas, A. Mikhailovsky, R. P. Raab, J. Liu, P. W. Blom, M. A. Loi, *et al.*, "Systematic study of exciton diffusion length in organic semiconductors by six experimental methods," Materials Horizons **1**, 280–285 (2014).

[8]J. R. Caram, S. Doria, D. M. Eisele, F. S. Freyria, T. S. Sinclair, P. Rebentrost, S. Lloyd, and M. G. Bawendi, "Room-temperature micron-scale exciton migration in a stabilized emissive molecular aggregate," Nano letters **16**, 6808–6815 (2016).

[9]A. Suna, "Kinematics of exciton-exciton annihilation in molecular crystals," Physical Review B **1**, 1716 (1970).

[10]Y. Firdaus, V. M. Le Corre, S. Karuthedath, W. Liu, A. Markina, W. Huang, S. Chattopadhyay, M. M. Nahid, M. I. Nugraha, Y. Lin, *et al.*, "Long-range exciton diffusion in molecular nonfullerene acceptors," Nature communications **11**, 5220 (2020).

[11]G. Bressan, M. Jirasek, H. L. Anderson, I. A. Heisler, and S. R. Meech, "Exciton–exciton annihilation as a probe of exciton diffusion in large porphyrin nanorings," The Journal of Physical Chemistry C **124**, 18416–18425 (2020).

[12]A. Steinhoff, F. Jahnke, and M. Florian, "Microscopic theory of exciton-exciton annihilation in two-dimensional semiconductors," Physical Review B **104**, 155416 (2021).

[13]V. Kenkre, "Theory of exciton annihilation in molecular crystals," Physical Review B **22**, 2089 (1980).

[14]A. Srivastava and J. Kono, "Diffusion-limited exciton-exciton annihilation in single-walled carbon nanotubes: A time-dependent analysis," Physical Review B—Condensed Matter and Materials Physics **79**, 205407 (2009).

[15]F. Fennel and S. Lochbrunner, "Exciton-exciton annihilation in a disordered molecular system by direct and multistep Förster transfer," Physical Review B **92**, 140301 (2015).

[16]P. Maly and T. Mancal, "Signatures of exciton delocalization and exciton–exciton annihilation in fluorescence-detected two-dimensional coherent spectroscopy," The Journal of Physical Chemistry Letters **9**, 5654–5659 (2018).

[17]T. Brixner, R. Hildner, J. Köhler, C. Lambert, and F. Würthner, "Exciton transport in molecular aggregates–from natural antennas to synthetic chromophore systems," Advanced Energy Materials **7**, 1700236 (2017).

[18]N. J. Hestand and F. C. Spano, "Expanded theory of H-and J-molecular aggregates: the effects of vibronic coupling and intermolecular charge transfer," Chemical reviews **118**, 7069–7163 (2018).

[19]S. King, D. Dai, C. Rothe, and A. Monkman, "Exciton annihilation in a polyfluorene: Low threshold for singlet-singlet annihilation and the absence of singlet-triplet annihilation," Physical Review B—Condensed Matter and Materials Physics **76**, 085204 (2007).

[20]F. Ito, T. Inoue, D. Tomita, and T. Nagamura, "Excited-state relaxation process of free-base and oxovanadium naphthalocyanine in near-infrared region," The Journal of Physical Chemistry B **113**, 5458–5463 (2009).

[21]I. G. Scheblykin, O. Y. Sliusarenko, L. S. Lepnev, A. G. Vitukhnovsky, and M. Van der Auweraer, "Strong nonmonotonous temperature dependence of exciton migration rate in J aggregates at temperatures from 5 to 300 K," The Journal of Physical Chemistry B **104**, 10949–10951 (2000).

[22]S. F. Volker, A. Schmiedel, M. Holzapfel, K. Renziehausen, V. Engel, and C. Lambert, "Singlet–singlet exciton annihilation in an exciton-coupled squaraine-squaraine copolymer: A model toward hetero-J-aggregates," The Journal of Physical Chemistry C **118**, 17467–17482 (2014).

[23]S. Kumar, I. S. Dunn, S. Deng, T. Zhu, Q. Zhao, O. F. Williams, R. Tempelaar, and L. Huang, "Exciton annihilation in molecular aggregates suppressed through quantum interference," Nature Chemistry **15**, 1118–1126 (2023).

[24]R. Khairutdinov and N. Serpone, "Photophysics of cyanine dyes: Subnanosecond relaxation dynamics in monomers, dimers, and H-and J-aggregates in solution," The Journal of Physical Chemistry B **101**, 2602–2610 (1997).

[25]M. F. Gelin, D. Egorova, and W. Domcke, "Exact quantum master equation for a molecular aggregate coupled to a harmonic bath," Physical Review E—Statistical, Nonlinear, and Soft Mat-

ter Physics **84**, 041139 (2011).
[26]K. Song, S. Bai, and Q. Shi, "A time domain two-particle approximation to calculate the absorption and circular dichroism line shapes of molecular aggregates," The Journal of Chemical Physics **143** (2015).
[27]T. Renger and V. May, "Theory of multiple exciton effects in the photosynthetic antenna complex LHC-II," The Journal of Physical Chemistry B **101**, 7232–7240 (1997).
[28]T. Renger and V. May, "Multiple exciton effects in molecular aggregates: Application to a photosynthetic antenna complex," Physical review letters **78**, 3406 (1997).
[29]S. Adhikari and R. Baer, "Stochastically bundled dissipators for the quantum master equation," Journal of Chemical Theory and Computation **21**, 4142–4150 (2025).
[30]P. A. M. Dirac, "The quantum theory of the emission and absorption of radiation," Proceedings of the Royal Society of London. Series A, Containing Papers of a Mathematical and Physical Character **114**, 243–265 (1927).
[31]C. Didraga and J. Knoester, "Excitons in tubular molecular aggregates," Journal of luminescence **110**, 239–245 (2004).
[32]C. Chuang, D. I. Bennett, J. R. Caram, A. Aspuru-Guzik, M. G. Bawendi, and J. Cao, "Generalized Kasha's model: T-dependent spectroscopy reveals short-range structures of 2d excitonic systems," Chem **5**, 3135–3150 (2019).
[33]A. P. Deshmukh, D. Koppel, C. Chuang, D. M. Cadena, J. Cao, and J. R. Caram, "Design principles for two-dimensional molecular aggregates using Kasha's model: tunable photophysics in near and short-wave infrared," The Journal of Physical Chemistry C **123**, 18702–18710 (2019).
[34]M. Müller, A. Paulheim, A. Eisfeld, and M. Sokolowski, "Finite size line broadening and superradiance of optical transitions in two dimensional long-range ordered molecular aggregates," The Journal of chemical physics **139** (2013).
[35]D. Abramavicius, B. Palmieri, D. V. Voronine, F. Sanda, and S. Mukamel, "Coherent multidimensional optical spectroscopy of excitons in molecular aggregates; quasiparticle versus supermolecule perspectives," Chemical reviews **109**, 2350–2408 (2009).
[36]D. Manzano, C. Chuang, and J. Cao, "Quantum transport in d-dimensional lattices," New Journal of Physics **18**, 043044 (2016).
[37]M. Steudtner and S. Wehner, "Fermion-to-qubit mappings with varying resource requirements for quantum simulation," New Journal of Physics **20**, 063010 (2018).
[38]N. C. Bradbury, C. Chuang, A. P. Deshmukh, E. Rabani, R. Baer, J. R. Caram, and D. Neuhauser, "Stochastically realized observables for excitonic molecular aggregates," The Journal of Physical Chemistry A **124**, 10111–10120 (2020).
[39]Y. Cytter, E. Rabani, D. Neuhauser, and R. Baer, "Stochastic density functional theory at finite temperatures," Physical Review B **97**, 115207 (2018).
[40]R. Baer, D. Neuhauser, and E. Rabani, "Stochastic vector techniques in ground-state electronic structure," Annual Review of Physical Chemistry **73**, 255–272 (2022).
[41]N. C. Bradbury, R. F. Ribeiro, J. R. Caram, and D. Neuhauser, "Stochastic methodology shows molecular interactions protect two-dimensional polaritons," Physical Review B **109**, L241303 (2024).
[42]M. Dahlbom, T. Minami, V. Chernyak, T. Pullerits, V. Sundström, and S. Mukamel, "Exciton-Wave Packet Dynamics in Molecular Aggregates Studied with Pump- Probe Spectroscopy," The Journal of Physical Chemistry B **104**, 3976–3983 (2000).
[43]Y. Wan, A. Stradomska, S. Fong, Z. Guo, R. D. Schaller, G. P. Wiederrecht, J. Knoester, and L. Huang, "Exciton level structure and dynamics in tubular porphyrin aggregates," The Journal of Physical Chemistry C **118**, 24854–24865 (2014).
[44]T. Jansen, L. M. Günther, J. Knoester, and J. Köhler, "Electronically excited states in cylindrical molecular aggregates: Exciton delocalization, dynamics, and optical response," Chemical Physics Reviews **5** (2024).
[45]R. Wang, C. Zhang, B. Zhang, Y. Liu, X. Wang, and M. Xiao, "Magnetic dipolar interaction between correlated triplets created by singlet fission in tetracene crystals," Nature communications **6**, 8602 (2015).
[46]W. Popp, D. Brey, R. Binder, and I. Burghardt, "Quantum dynamics of exciton transport and dissociation in multichromophoric systems," Annual review of physical chemistry **72**, 591–616 (2021).
[47]R. Tempelaar and T. C. Berkelbach, "Many-body simulation of two-dimensional electronic spectroscopy of excitons and trions in monolayer transition metal dichalcogenides," Nature communications **10**, 3419 (2019).
[48]A. Z. Lieberherr, J. Kelly, J. E. Runeson, T. E. Markland, and D. E. Manolopoulos, "Two-dimensional electronic spectra from trajectory-based dynamics: Pure-state ehrenfest, spin-mapping, and mean classical path approaches," The Journal of Chemical Physics **163** (2025).
[49]M. Kasha, H. R. Rawls, and M. A. El-Bayoumi, "The exciton model in molecular spectroscopy," Pure and applied Chemistry **11**, 371–392 (1965).
[50]M. Kasha, "Energy transfer mechanisms and the molecular exciton model for molecular aggregates," Radiation research **20**, 55–70 (1963).
[51]E. G. McRae and M. Kasha, "Enhancement of phosphorescence ability upon aggregation of dye molecules," The Journal of Chemical Physics **28**, 721–722 (1958).
[52]M. Kasha, "Relation between exciton bands and conduction bands in molecular lamellar systems," Reviews of Modern Physics **31**, 162 (1959).
[53]D. Abramavicius and S. Mukamel, "Exciton dynamics in chromophore aggregates with correlated environment fluctuations," The Journal of chemical physics **134** (2011).
[54]V. Czikklely, H. Forsterling, and H. Kuhn, "Extended dipole model for aggregates of dye molecules," Chemical Physics Letters **6**, 207–210 (1970).
[55]I. Ryzhov, G. Kozlov, V. Malyshev, and J. Knoester, "Low-temperature kinetics of exciton–exciton annihilation of weakly localized one-dimensional Frenkel excitons," The Journal of Chemical Physics **114**, 5322–5329 (2001).
[56]E. R. Bittner and C. Silva, "Concerning the stability of biexcitons in hybrid HJ aggregates of π-conjugated polymers," The Journal of Chemical Physics **156** (2022).
[57]J. Hubbard, "Electron correlations in narrow energy bands," Proceedings of the Royal Society of London. Series A. Mathematical and Physical Sciences **276**, 238–257 (1963).
[58]E. Gutiérrez-Meza, R. Malatesta, H. Li, I. Bargigia, A. R. Srimath Kandada, D. A. Valverde-Chávez, S.-M. Kim, H. Li, N. Stingelin, S. Tretiak, *et al.*, "Frenkel biexcitons in hybrid HJ photophysical aggregates," Science advances **7**, eabi5197 (2021).
[59]M. F. Hutchinson, "A stochastic estimator of the trace of the influence matrix for Laplacian smoothing splines," Communications in Statistics-Simulation and Computation **18**, 1059–1076 (1989).
[60]A. V. Bobylev and T. Ohwada, "The error of the splitting scheme for solving evolutionary equations," Applied mathematics letters **14**, 45–48 (2001).
[61]A. P. Deshmukh, N. Geue, N. C. Bradbury, T. L. Atallah, C. Chuang, M. Pengshung, J. Cao, E. M. Sletten, D. Neuhauser, and J. R. Caram, "Bridging the gap between H-and J-aggregates: Classification and supramolecular tunability for excitonic band structures in two-dimensional molecular aggregates," Chemical Physics Reviews **3** (2022).
[62]C. Didraga and J. Knoester, "Exchange narrowing in circular and cylindrical molecular aggregates: degenerate versus nondegenerate states," Chemical physics **275**, 307–318 (2002).
[63]M. Van der Auweraer and I. Scheblykin, "One-dimensional J-aggregates: Dependence of the properties of the exciton band on the model of the intermolecular coupling," Chemical physics **275**, 285–306 (2002).
[64]S. Valleau, S. K. Saikin, M.-H. Yung, and A. A. Guzik, "Exciton transport in thin-film cyanine dye J-aggregates," The journal of chemical physics **137** (2012).

[65]F. C. Spano and E. S. Manas, "Theory of coherent transient spectroscopy in molecular aggregates: The effects of interacting excitons," The Journal of chemical physics **103**, 5939–5955 (1995).

[66]J. M. Womick, S. A. Miller, and A. M. Moran, "Correlated exciton fluctuations in cylindrical molecular aggregates," The Journal of Physical Chemistry B **113**, 6630–6639 (2009).

[67]Z. Yu, M. Berding, and H. Wang, "Spatially correlated fluctuations and coherence dynamics in photosynthesis," Physical Review E—Statistical, Nonlinear, and Soft Matter Physics **78**, 050902 (2008).

[68]J. R. Caram, H. Zheng, P. D. Dahlberg, B. S. Rolczynski, G. B. Griffin, A. F. Fidler, D. S. Dolzhnikov, D. V. Talapin, and G. S. Engel, "Persistent interexcitonic quantum coherence in CdSe quantum dots," The journal of physical chemistry letters **5**, 196–204 (2014).

[69]G. Panitchayangkoon, D. Hayes, K. A. Fransted, J. R. Caram, E. Harel, J. Wen, R. E. Blankenship, and G. S. Engel, "Long-lived quantum coherence in photosynthetic complexes at physiological temperature," Proceedings of the National Academy of Sciences **107**, 12766–12770 (2010).

[70]M. Schröter, S. D. Ivanov, J. Schulze, S. P. Polyutov, Y. Yan, T. Pullerits, and O. Kühn, "Exciton–vibrational coupling in the dynamics and spectroscopy of Frenkel excitons in molecular aggregates," Physics Reports **567**, 1–78 (2015).

[71]A. Carta, B. Wittmann, K. Kreger, H.-W. Schmidt, T. L. Jansen, and R. Hildner, "Spatial correlations drive long-range transport and trapping of excitons in single H-aggregates: Experiment and theory," The Journal of Physical Chemistry Letters **15**, 2697–2707 (2024).

Supplementary Information for: Stochastic Evaluation of Exciton–Exciton Annihilation Rate in 2D Molecular Aggregate

1 Deterministic method for computing EEA rate

Within the deterministic direct diagonalization approach, the exciton–exciton annihilation rate is evaluated from Fermi's golden rule,

$$\Gamma = \frac{2\pi}{\hbar\gamma} \sum_{\lambda} P_{\lambda} \sum_{m} \left| \langle S(m) | H_a | \Psi_{\lambda} \rangle \right|^2 , \tag{1}$$

with all parameters defined in the main text.
Using the two-exciton expansion

$$|\Psi_{\lambda}\rangle = \sum_{m<n} C_{\lambda}(m,n)\, |m,n\rangle, \tag{2}$$

and writing the annihilation Hamiltonian in the mixed one-/two-exciton basis as

$$H_a = \sum_{m \neq n} V_{m,n}\, |m\rangle\langle m,n| + \text{H.c.}, \tag{3}$$

its action on a two-exciton eigenstate is

$$H_a |\Psi_{\lambda}\rangle = \sum_{m<n} V_{m,n}\, C_{\lambda}(m,n)\, |m\rangle. \tag{4}$$

Projecting onto the localized final state $|S(m)\rangle = |m\rangle$ gives

$$\langle S(m) | H_a | \Psi_{\lambda} \rangle = \sum_{n>m} V_{m,n}\, C_{\lambda}(m,n). \tag{5}$$

Substituting this matrix element into Fermi's golden rule yields the direct diagonalization expression for the EEA rate,

$$\Gamma = \frac{2\pi}{\hbar\gamma} \sum_{\lambda} P_{\lambda} \sum_{m} \left| \sum_{n>m} V_{m,n}\, C_{\lambda}(m,n) \right|^2 . \tag{6}$$

With the working approximation

$$V_{m,n} = \alpha J_{m,n}, \tag{7}$$

this becomes

$$\Gamma = \frac{2\pi}{\hbar\gamma} \sum_{\lambda} P_{\lambda} \sum_{m} \left| \sum_{n>m} \alpha J_{m,n}\, C_{\lambda}(m,n) \right|^2 \tag{8}$$

This is the form used in the direct diagonalization calculations [1, 2].

2 Benchmark k_{stoch} and n_{step} against deterministic direct diagonalization

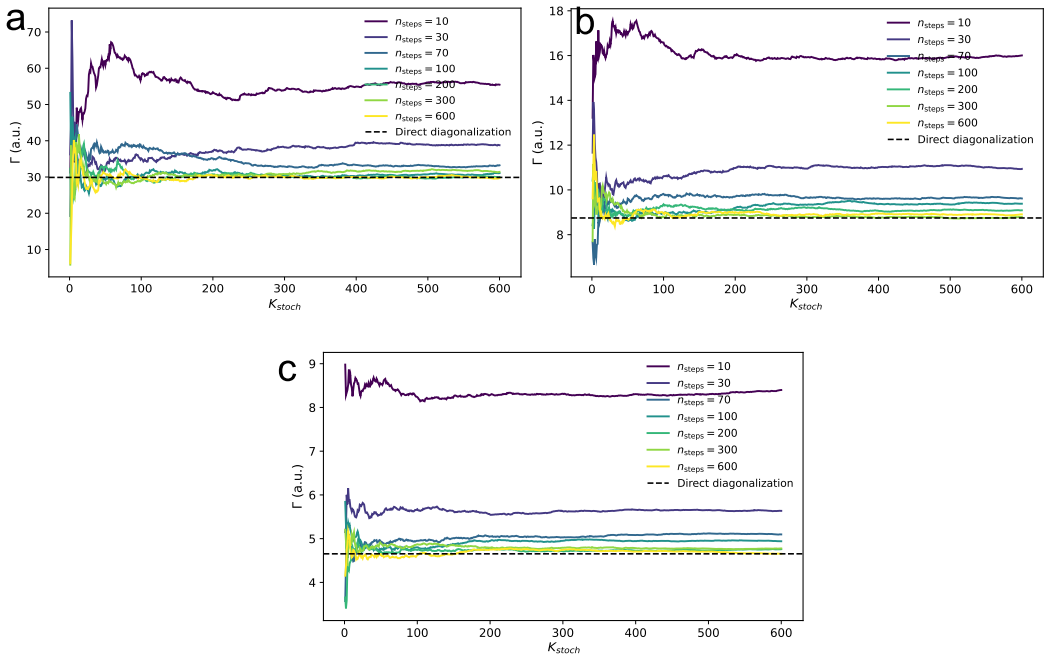

Figure S1: Convergence of the stochastic estimate of the EEA rate at slip = 0 Å as a function of k_{stoch} and n_{step} for aggregates of increasing size: (a) $N_x = N_y = 3$, (b) $N_x = N_y = 9$, and (c) $N_x = N_y = 13$. The temperature was set to be 300K when computing all of these results.

To validate the stochastic method, we compared the EEA rates with deterministic results obtained by direct matrix diagonalization for different system sizes, as shown in Figure S1 a-c. By systematically varying k_{stoch} and n_{step}, we found that at slide = 0 Å, $k_{\text{stoch}} = 300$ and $n_{\text{step}} = 300$ are sufficient to achieve convergence.

3 Model Parameters for 2D Aggregates

The geometrical and electronic parameters of the 2D aggregates are chosen to be representative of commonly studied 2D cyanine dye(Cy3) aggregates reported in this literature [3].
Each monomer is modeled as a rectangular unit with an effective length of 16 Å and width of 4 Å, defining the underlying lattice geometry. The transition dipole is represented using the extended dipole model with a charge separation distance of $d = 4$ Å. The magnitude of the transition dipole moment is taken to be $\mu = 2.5$ D.

4 Slip-Dependent Excitonic Regimes

The dependence of excitonic properties on the intermolecular slip parameter is illustrated in Figure S2. The slip controls the relative arrangement of transition dipoles and therefore strongly modulates the electronic coupling, leading to distinct excitonic regimes.

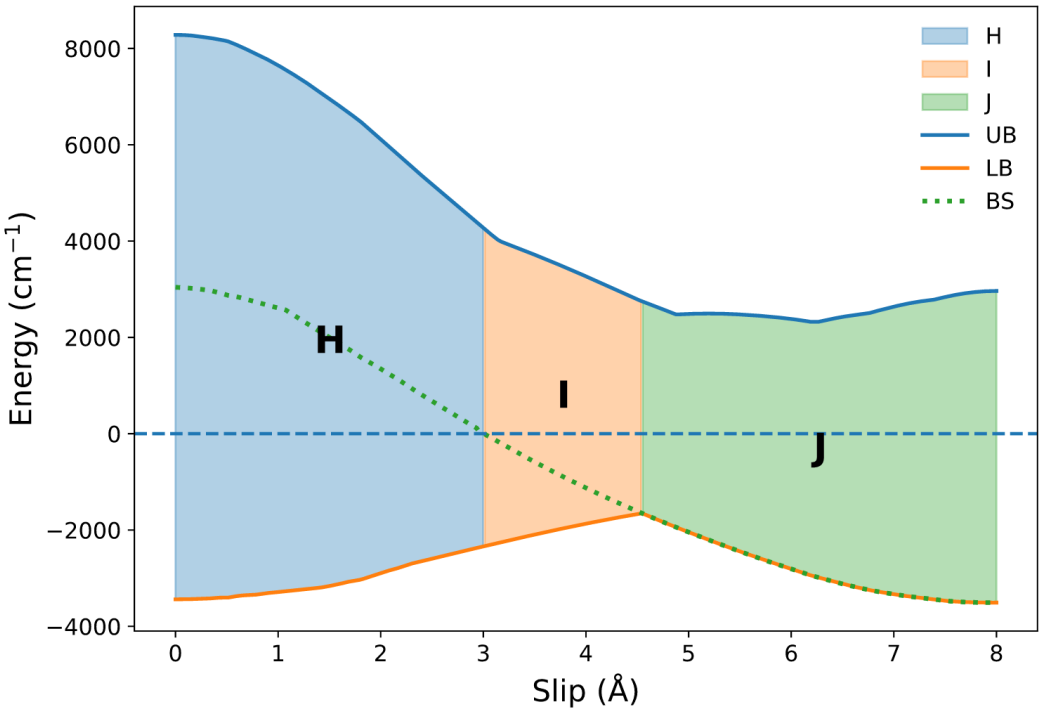

Figure S2: Slip dependence of the exciton band structure.

At small slip ($s \lesssim 3.0$Å), the aggregate is H-like, where positive short-range couplings dominate over the always-negative long-range contributions, placing the bright state above the monomer with a blue-shifted transition. As slip increases, the system enters an intermediate (I) regime near $s \approx 3.5$Å,

where short- and long-range couplings compete and partially cancel, yielding an overall negative coupling but a bright state that remains away from the band edge. At larger slip ($s \gtrsim 4.6$Å), both short- and long-range couplings are negative, producing a band-edge bright state characteristic of J-aggregation with a red-shifted transition.

5 Microscopic Origin of the Increased EEA Rate with κ in J-Aggregates

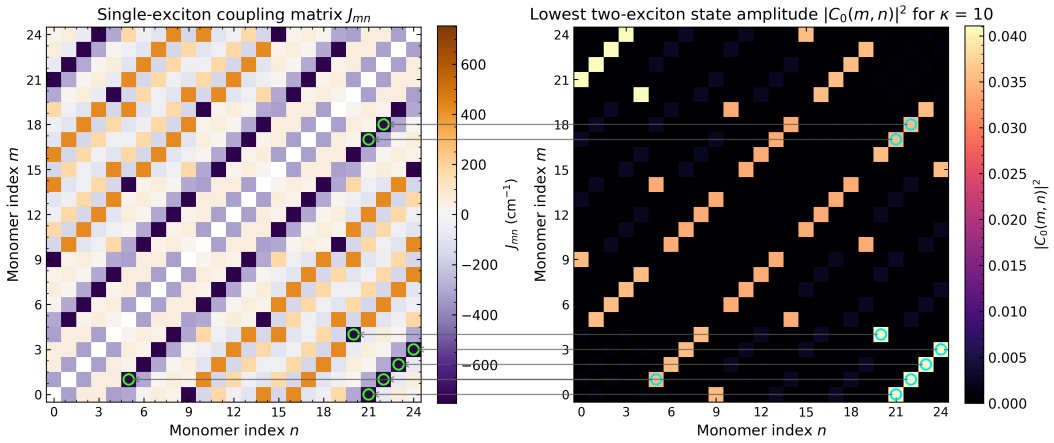

Figure S3: Correlation between pair coupling and localization in the lowest two-exciton state. The system is adapted as a toy model J aggregate with $N_x = N_y = 5$ and slip = 6.5 Å for illustrative purposes.

To examine the increase in the EEA rate with increasing κ in J-aggregates, we analyze the relationship between the coupling matrix elements J_{mn} and the lowest-energy two-exciton state (Figure S3). We found that the dominant amplitudes of the lowest-energy two-exciton wavefunction are concentrated on basis states for which J_{mn} is strongly negative, while the corresponding coefficients $C_n(m,n)$ are also large. As a result, the matrix element

$$\left| \sum_{n>m} \alpha J_{m,n} \, C_\lambda(m,n) \right|^2$$

becomes significantly enhanced and hence the EEA rate. This correlation can be seen directly from the arrows in Figure S3.

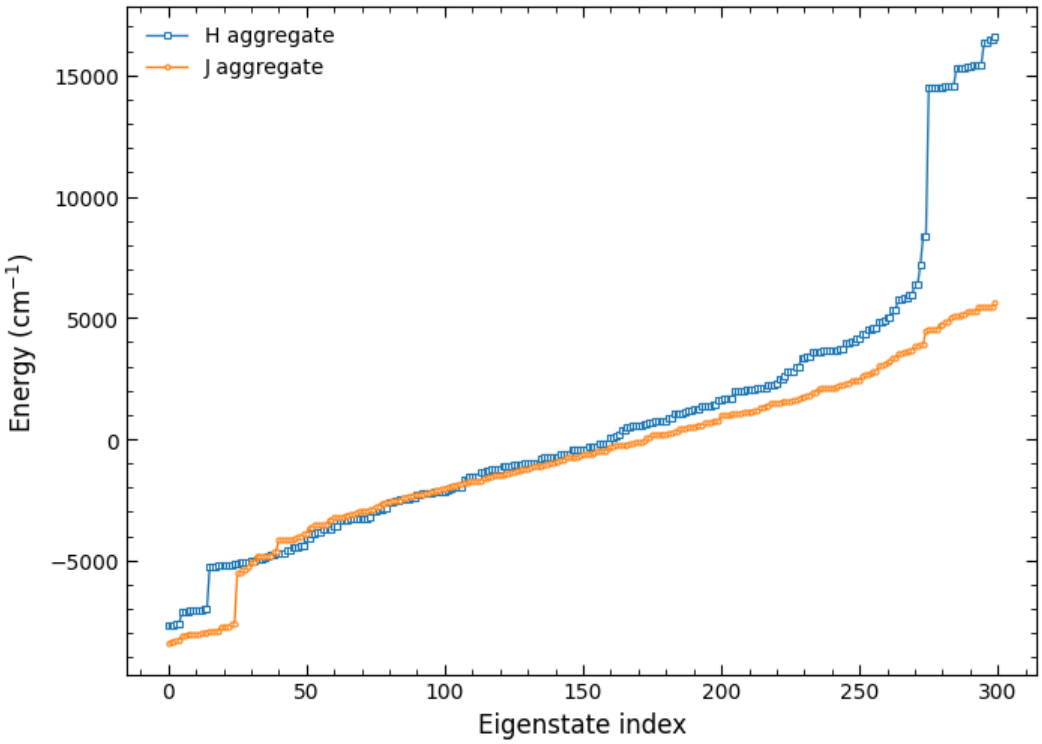

Figure S4: Eigenenergy spectrum for J and H aggregates. The system is adapted as a toy model J and H aggregate with $\kappa = 10$, $N_x = N_y = 5$, slip = 6.5 Å and = 2.5 Å respectively for illustrative purposes.

We then examined the two-exciton eigenenergy spectra of the J- and H-aggregates using deterministic calculations(Figure S3). The spectra clearly reveal localized gap states near the band edges in both systems: at the lower-energy edge for the J-aggregate and at the higher-energy edge for the H-aggregate. These states resemble disorder-induced gap states. In the J-aggregate, the presence of such low-energy gap states effectively suppresses thermal access to higher-energy two-exciton states, thereby enhancing the EEA rate.[4] By contrast, in the H-aggregate, although similar states appear near the upper band edge, they are only accessible at very high temperatures and thus have a much smaller effect on the annihilation dynamics.

References

[1] Sarath Kumar, Ian S Dunn, Shibin Deng, Tong Zhu, Qiuchen Zhao, Olivia F Williams, Roel Tempelaar, and Libai Huang. Exciton annihilation in molecular aggregates suppressed through quantum interference. *Nature Chemistry*, 15(8):1118–1126, 2023.

[2] Roel Tempelaar, Thomas LC Jansen, and Jasper Knoester. Exciton–exciton annihilation is coherently suppressed in H-Aggregates, but not in

J-aggregates. *The journal of physical chemistry letters*, 8(24):6113–6117, 2017.

[3] Arundhati P Deshmukh, Niklas Geue, Nadine C Bradbury, Timothy L Atallah, Chern Chuang, Monica Pengshung, Jianshu Cao, Ellen M Sletten, Daniel Neuhauser, and Justin R Caram. Bridging the gap between H-and J-aggregates: Classification and supramolecular tunability for excitonic band structures in two-dimensional molecular aggregates. *Chemical Physics Reviews*, 3(2), 2022.

[4] Eric R Bittner and Carlos Silva. Concerning the stability of biexcitons in hybrid HJ aggregates of π-conjugated polymers. *The Journal of Chemical Physics*, 156(18), 2022.